An Individual Nanocube-Based Plasmonic Biosensor for Real-Time Monitoring the Structural Switch of the Telomeric G-Quadruplex

Yuanyuan Tian, Lei Zhang, Jingjing Shen, Lingzhi Wu, Hongzhang He, Dik-Lung Ma, Chung-Hang Leung, Weibing Wu, Quli Fan, Wei Huang, and Lianhui Wang**

***P**romoted by the localized surface plasmon resonance nanotechnology, a simple and sensitive plasmonic aptamer nanosensor (nanoaptasensor) on an individual Au@Ag core-shell nanocube (Au@Ag NC) has been proposed for real-time monitoring of the formation process of G-quadruplex structures and label-free analysis of potassium ions (K^+). In particular, the analysis of the thermodynamic parameters indicates that there are two types of binding states accompanied with a remarkable change of free energy (ΔG) in the sequential folding process of telomere DNA sequence. This nanoaptasensor has raised promising applications in monitoring the dynamic process of the structural switch of the G-quadruplex.*

1. Introduction

Due to the localized surface plasmon resonance (LSPR) effect, the noble metal nanoparticles exhibit unique optical and physical properties, such as plasmon resonance scattering, coupling effect, and Raman scattering, which have attracted considerable attention in recent decades for a variety of applications, including biological imaging, phototherapy, optical data storage, and sensing technologies.[1] Arising from the coherent oscillation of the conduction electrons in the conduction band of noble metal nanocrystals, LSPR strongly depends on the nanocrystal morphology, surrounding dielectric environment, size of the nanoparticle, and the wavelength of the light when excited by incident radiation.[2] The advent

Y. Y. Tian, Prof. L. Zhang, J. J. Shen, Prof. L. Z. Wu, Prof. Q. L. Fan, Prof. W. Huang, Prof. L. H. Wang
Key Laboratory for Organic Electronics and Information Displays & Institute of Advanced Materials (IAM)
National Jiangsu Synergetic Innovation Center for Advanced Materials (SICAM)
Nanjing University of Posts & Telecommunications
9 Wenyuan Road, Nanjing 210023, China
E-mail: iamqlfan@njupt.edu.cn; iamlhwang@njupt.edu.cn

Dr. H. Z. He, Prof. D.-L. Ma
Department of Chemistry
Hong Kong Baptist University
Kowloon Tong, Hong Kong, China

Prof. C.-H. Leung
State Key Laboratory of Quality Research in Chinese Medicine
Institute of Chinese Medical Sciences
University of Macau
Macao, China

Prof. W. B. Wu
Jiangsu Provincial Key Lab of Pulp and Paper Science and Technology
Nanjing Forestry University
Nanjing 210037, China

Prof. W. Huang
Key Laboratory of Flexible Electronics (KLOFE) & Institute of Advanced Materials (IAM)
National Jiangsu Synergetic Innovation Center for Advanced Materials (SICAM)
Nanjing Tech University
30 South Puzhu Road, Nanjing 211816, China

DOI: 10.1002/smll.201600041

of LSPR scattering spectroscopy based on dark-field microscopy (DFM) has enabled the study of the local environment of a single plasmonic nanoparticle, which further facilitates its use in biological labeling and detection[3] by adsorption,[4] plasmon resonance energy transfer,[5] coupling effect,[6] and the refractive index (RI) changing around the particles.[7]

The telomere aptamer is a nucleic acid ligand that binds to specific target molecules with high affinity and specificity, presenting the advantages such as easy modification, high selectivity, good stability, target versatility, and easy storage, and has been used as a novel sensing and recognition element to detect bacteria, macromolecules, small molecules, and metal ions.[5c] Furthermore, telomere aptamer sequences with cyclic hydrogen bonding of four guanines can fold into a secondary structure of the DNA tetraplex via intramolecular hydrogen bonding interactions.[9] G-quadruplex formation is promoted in the presence of univalent cations, such as Na^+, K^+, Pb^{2+}, Sr^{2+}, and ATP, which are coordinated to the guanine O_6 carbonyl groups among the planes of neighboring quartets.[10] Compared with the cavities within G-quadruplex, the complementary size and charge of K^+ provide a rationale for the observation that K^+ stabilizes such structures much more strongly than other monovalent cations.[11] Potassium ions play key roles in biological systems, such as extracellular osmolarity, nerve transmission, regulation of blood pressure, pH, enzyme activation, apoptosis of a cell, and the formation of collagen or elastin.[12] Despite extensive investigations of the applications of G-quadruplex in colorimetric, fluorescence and electrochemistry, it is difficult to perform as nanoscale sensors with high sensitivity and optical stability for trace analysis.[13,14] Therefore, it is important to develop a selective and sensitive method for the detection of potassium ions for medical diagnosis and nutritional analysis at nanoscale dimensions.

In our previous studies, the hybridization of target nucleic acid and probe molecules on an individual gold nanoparticle surface induced a change in the dielectric constant in the surrounding microenvironment, which resulted in a notable redshift of the LSPR peak position.[7a] Moreover, a single silver nanocube-based LSPR nanosensor has been employed for the detection of the trace lung cancer-associated microRNAs with ultrasensitivity.[7b] The RI of the microenvironment changed delicately when DNA or RNA hybridized near a single DNA-capped nanoparticle surface.[7c] In this work, as-prepared Au@Ag nanocube (NC) conjugated with telomere aptamer is chosen as the core material owing to the advantages of sensitive sensing and a detectable color change accompanying the redshift in its extinction spectrum. In addition, G-quadruplex formed from this telomere aptamer can not only be used as a detection platform for the dynamic formation process but also as a target for the label-free analysis of metal ions. In this respect, for the first time, a novel nanoaptasensor based on an individual nanoparticle has been fabricated for real-time monitoring of the dynamic formation process of G-quadruplex structures and label-free analysis of K^+.

A schematic representation of a nanoaptasensor is displayed in **Figure 1**a. Au@Ag NCs were immobilized on the cleaned indium tin oxide (ITO) glass surface by physisorption, and every individual nanoparticle scatters strong blue light (Figure 1c) and the LSPR spectra (Figure 1d) could be easily observed with the help of a dark-field condenser. The nanoaptasensor was prepared as follows: (1) Immobilization of Au@Ag NCs on a cleaned ITO glass slide; (2) self-assembly of the aptamer on the surface of the Au@Ag NCs; (3) addition of K^+ onto the modified ITO glass side.

In this paper, a single strand DNA (ssDNA) sequence of the aptamer 5′-TTTTTTTTTT$(GGGTTA)_3$GGGTTTTTTTTTT-3′-$(CH_2)_6$–SH, in which a G-rich specific sequence offered a unique K^+ binding site in the intramolecular tetraplex, was linked to the Au@Ag NCs surface by Ag—S covalent bond. The aptamer adopted a random-coil structure in the absence of potassium and could switch to the G-quartet formation complex in K^+ solution.[12b,15] In general, G-quadruplex DNA has much more space-to-charge density than ssDNA, because the persistent length of random coil ssDNA with 41 bases is about 17.0 nm and that of a more condensed G-quadruplex DNA is only about 9.7 nm.[13a] Compared with the random

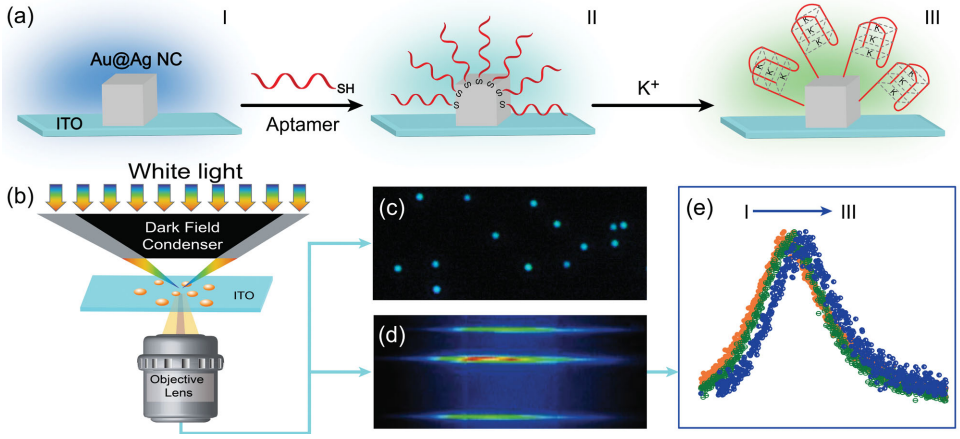

Figure 1. a) Schematic representation of the K^+ nanoaptasensor. It displays the mechanism of the structural transition during sensing of a G-rich aptamer from a random coil to G-quadruplex induced by K^+. b) Diagram of a single particle sensor platform with DFM. c) A typical DFM image of Au@Ag NCs modified on a microscopy glass slide. d) Corresponding LSPR spectra of single Au@Ag NC in a slit. e) Showing LSPR scattering spectra of the individual Au@Ag NC sensor at step I, II, and III in panel (a).

coil ssDNA, the G-quadruplex structure possesses a larger RI around an individual nanocube. The addition of K^+ induces the DNA structure switching, resulting in a delicate increase of RI which leads to a notable redshift of the scattering spectra (Figure 1e).

Figure 2. a) TEM images of Au@Ag NCs. b) DFM image of the Au@Ag NCs on an ITO glass slide. c) In situ SEM image of the selected area Au@Ag NCs in DFM image (insert: the enlarged SEM image).

2. Results and Discussion

2.1. Structure and Morphology of Au@Ag NCs

For the accuracy of quantitative analysis for tracking bioprocesses in a slight space-to-charge, the nanoparticle with good monodispersity is required to obtain a stable peak position of LSPR scattering spectra due to the LSPR spectral sensitivity which is highly dependent on their size and geometrical parameters of plasmonic nanoparticles. Recently, theoretical simulations and experimental data have demonstrated that anisotropic nanostructures exhibit higher RI sensitivity than spherical nanoparticles.[1a,16] The unique optical properties of gold nanorods mainly dependent on its different aspect ratios, but it is difficult to control the aspect ratios in the synthesis process, which lead to a large range of LSPR peak position distribution in 80 nm.[17] The individual varieties hinder prospects of further application in quantitative analysis of the plasmonic nanobiosensor, especially for judging the conformational change on different individual nanoparticle. Despite the superior sensitivity of silver cubes, its high reactivity which is susceptible to corrosion in aqueous environments and oxidation in air make it less popular for sensing molecules in complex biological samples.[18]

The monodisperse Au@Ag nanocubes were synthesized in a facile and mature route with relatively high yield (86%–90%) in an aqueous solution as reported by Xia and coworkers.[19] A seed-mediated growth process was employed to prepare the Au@Ag NCs with better monodispersity than Ag cubes in aqueous suspension.[7b,20] These Au@Ag nanocubes with highly tunable and controllable sizes and shell thicknesses (Figure S1, Supporting Information) allowed us to synthesize readily and investigate systematically their LSPR properties (Figure S2, Supporting Information). It is worth noting that large plasmonic particle tend to induce a peak broadening of plasmon resonance, which lead to a lower signal-noise ratio.[1a,16b] To ensure a sufficient light-scattering signal with a high absorption cross-section and dominant scattering character, the size of the Au@Ag NCs 51.2 nm was employed to fabricate optical plasmonic nanoaptasensor. The range of LSPR peak position distribution is only 15 nm (Figure S2, Supporting Information), which can improve the accuracy of quantitative analysis by plasmonic sensor with good monodisperse Au@Ag NCs. From the TEM images of Au@Ag NCs in **Figure 2**a, it is clear that essentially every cube contained one Au nanocrystal seed in its center. An obvious difference in contrast can be observed between the Au core and the Ag shell because of the difference in atomic number and thus attenuation of electrons. Figure 2b shows the DFM image of several Au@Ag NCs on the ITO glass slide. Every blue spot is attributed to the Au@Ag NC's strong plasmonic scattering effect, and every Au@Ag NC exhibits strong light scattering at ≈495–510 nm. From the enlarged SEM image (Figure 2c, inset) and the corresponding LSPR scattering spectra (Figure S3, Supporting Information) of the Au@Ag NCs in the corresponding selected area completely in Figure 2b, we can conclude that the peak position and the full width at half maximum of the scattering spectra depend on the NC's shape and size. Because of the strong coupling effect between these nanoparticles, they exhibited another color (green, yellow or white spot) if there were more than two NCs aggregated together (Figure S4, Supporting Information).

2.2. Fabrication of Nanoaptasensor

An individual Au@Ag NC with an initial scattering peak around 504 nm was employed to monitor the thiol-capping process in a 1×10^{-9} M aptamer solution. After modifying aptamer, the thiol-capping process on the surface of the NC results in a redshift of the LSPR scattering spectra of the Au@Ag NC (**Figure 3**a). Before reaching the saturation state, more aptamers were bound to the surface of the nanoparticle with extension of the modification time. The real-time dynamic process of the modification process was recorded continuously, and the LSPR scattering spectra peak position redshifted up to 518.4 nm (Figure 3b). In order to achieve a high performance nanoaptasensor, different modification time (0.5, 1, 2, 4, and 13 h) of the aptamer with Au@Ag NC were tested.

Figure 3c shows the intensity of the response signals of the nanoaptasensors, which are reflected in $\Delta\lambda_{max}$ changes (1.5, 2.5, 10.8, 4.2, and 3.1 nm). The result illustrates that as the modification time is extended, a higher density of probe molecules will inhibit the G-quadruplex formation due to steric hindrance. This procedure could also be repeated both in ultrapure water and 10×10^{-3} M PBS buffer (pH = 7.4) with good stability (Figure S5, Supporting Information). Accordingly, the optimum modification time was chosen as 2 h. The scattering peak of the nanoaptasensor is about 516 nm, and then it redshifts continuously to 526.8 nm in 10×10^{-3} M PBS containing 10×10^{-6} M K^+, and the $\Delta\lambda_{max}$ statistical data conform to Gaussian distributions, as shown in Figure 3d. The typical DFM images of the nanoaptasensors demonstrate whether the K^+ exists or not (Figure S6, Supporting Information). This exciting discovery suggests that the analysis of the LSPR spectra is an efficient method for the study of the

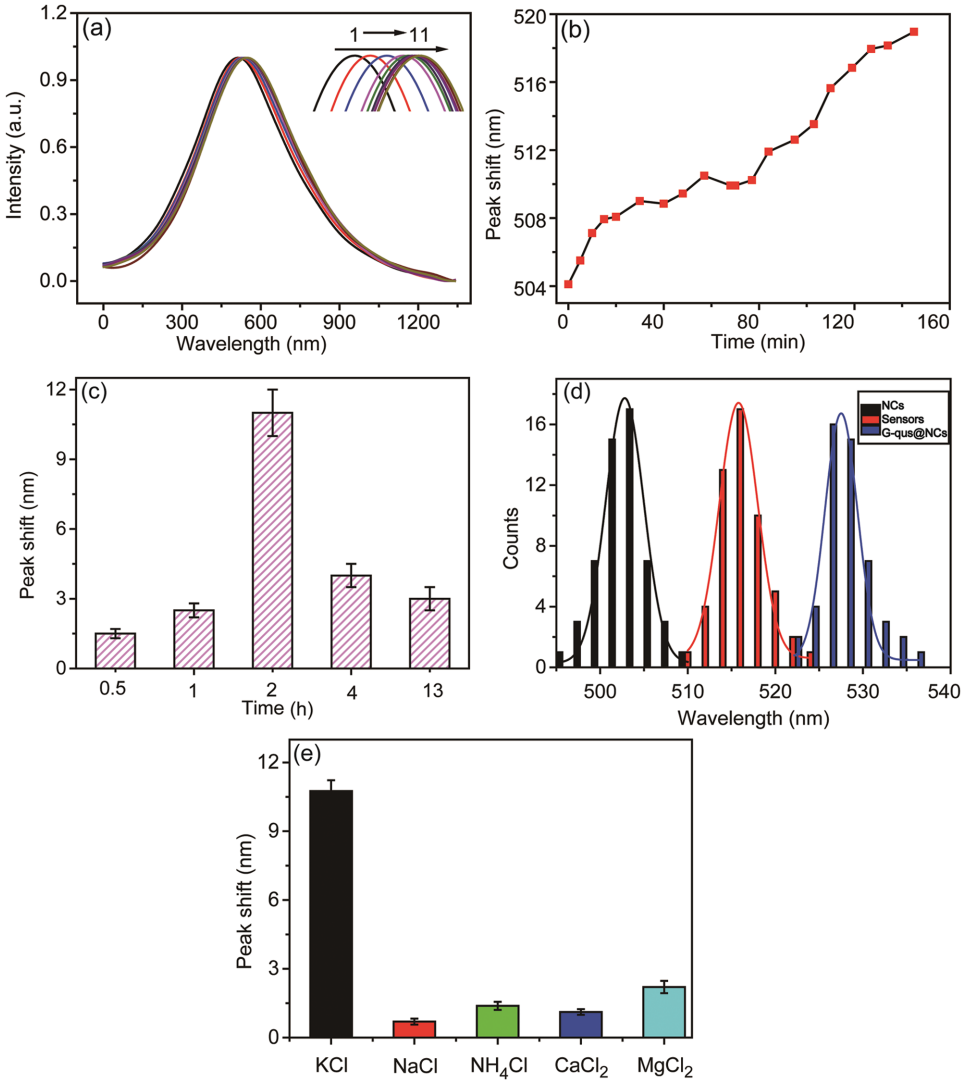

Figure 3. a) Representative time-dependence of an individual nanoaptasensor scattering spectra at different times after treatment with 1×10^{-9} M aptamer, showing that the LSPR spectra peaks are redshifted, spectra 1–11: 0, 8, 18, 30, 42, 55, 69, 85, 100, 110, 120 min (the scattering intensities of all the spectra have been normalized). b) Time-dependent LSPR scattering peak redshift of the aptamer modified with a single Au@Ag NC monitored over 2 h. c) LSPR scattering shifts of the nanoaptasensors with $K^+ = 10 \times 10^{-6}$ M, obtained at different time intervals after modification of the aptamer with Au@Ag NCs: 0.5, 1, 2, 4, and 13 h. d) Statistical analysis of the scattering spectra of Au@Ag NCs (black), nanoaptasensor with modified time 2 h (red) and the nanoaptasensor treated with 10×10^{-6} M K^+ (blue). e) Nanoaptasensor LSPR response of other cations (at 10×10^{-6} M).

specific reaction between aptamers and target molecules on a nanoparticle surface. Furthermore, it could also be used to design novel plasmonic sensors for biological-labeling or label-free detection with high sensitivity on an individual Au@Ag NC. To evaluate the selectivity of this nanoaptasensor, four interfering cations, Na^+, NH_4^+, Ca^{2+}, and Mg^{2+} were used (Figure 3e). Compared with the redshift of the LSPR peak in a K^+ solution, a small redshift of the scattering spectra was observed in the solutions containing other cations. This implies that the nanoaptasensor can recognize the target K^+ with high selectivity.

2.3. Analysis of K^+ and Gibbs Free Energy

To determine the sensitivity and evaluate the applicability of this method, time-depended LSPR spectra of nanoaptasensors with similar initial peak positions were recorded in different concentrations of K^+. It is worth mentioning that the redshift of scattering spectra peaks reaches a maximum value rapidly and then keeps a dynamic conformational equilibrium in which the immobilized aptamer is in the unfolded and folded state (**Figure 4**a). There is an upward tendency of the balance of reached time from 10 to 21 min, contrary to the increasing K^+ concentrations. The tendency that all the peak redshifts eventually reach a dynamic conformational equilibrium state indicates that the aptamer–K^+ reaction is self-confined around the nanoparticle. Furthermore, the results of binding rate and the $\Delta\lambda$ of the LSPR scattering peak increase with the concentration of K^+ (10^{-7}–10^{-3} M), where $\Delta\lambda$ = 2.81, 6.67, 10.74, 13.98 and 14.74 nm, respectively. The peak redshift reaches a maximum value rapidly to a saturated state when the concentration of K^+ is above 10^{-3} M, because the number of aptamer conjugated on the surface of

small NANO MICRO

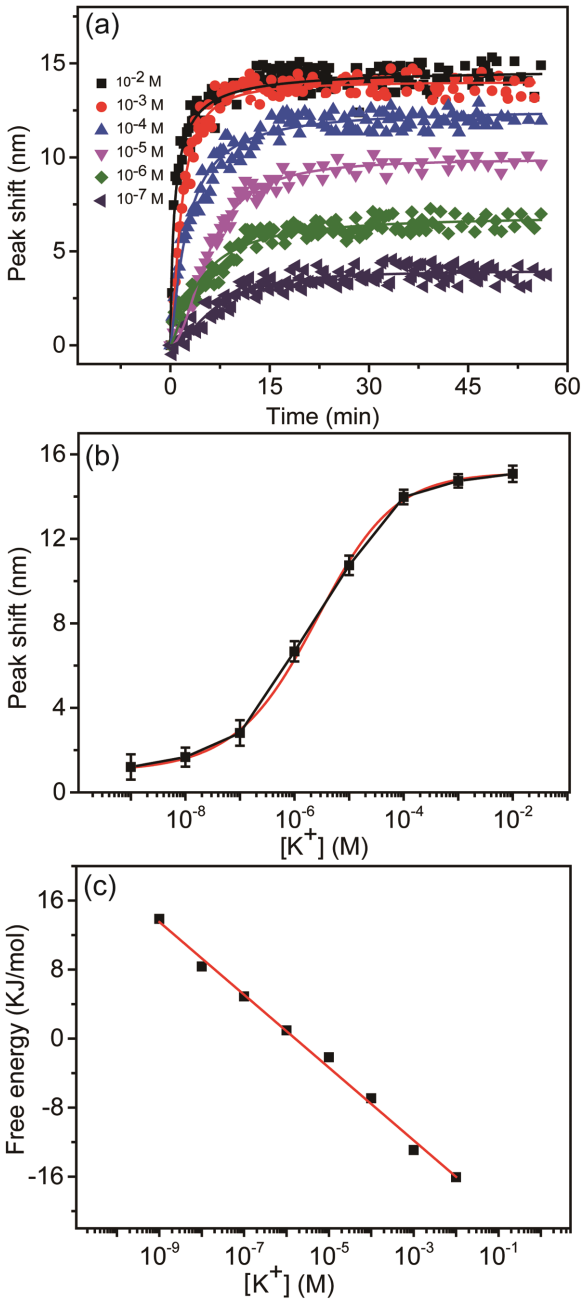

Figure 4. a) Measured (signs) and calculated (lines) time-dependent spectral shifts of the nanoaptasensors exposed to different concentrations of K^+. b) Relationship of the LSPR spectra peak shift ($\Delta\lambda$) in different concentrations of K^+ and fitting curve (red). c) Free energy change (ΔG) versus the K^+ concentration for the folding transition of G-quadruplex.

individual nanoparticle are constant on Au@Ag NCs surface after optimum modification time. During the binding interaction, there is a change in the amplitude of redshifts because dissociation occurs during the measurement time and some binding sites may be occupied multiple times. It is estimated that the binding rate may be controlled by K^+ diffusion of the local environment around the nanoaptasensor. The relationship between K^+ concentration and peak redshift $\Delta\lambda_{max}$ is estimated as follows

$$f(\lambda) = \frac{f(\lambda_{max}) C_{K^+}^n}{\left(K_d^n + C_{K^+}^n\right)^2} \quad (1)$$

Here K_d is the dissociation constant for high affinity sites, the n value is the binding stoichiometry, λ_{max} is the LSPR peak shift and C_{K^+} is the concentration of K^+. In the state of equilibrium, the dissociation constant $K_d = 2.16 \times 10^{-6}$ M could be calculated directly from Equation (1), which is a bit lower than the previously reported value, $K_d = 6 \pm 3 \times 10^{-6}$ M for the aptamer potassium complex.[10b,21] The main reason for this result, presumably, is the strong electrostatic attraction between the Au@Ag nanoaptasensor and K^+. The binding stoichiometry (n) of the affinity sites increases with the concentration of K^+ (10^{-7}–10^{-2} M), where $n = 0.89, 1.27, 1.37, 1.49, 1.87, 2.01$, respectively. Low affinity sites have a stoichiometry $n = 1.05 \pm 0.1$ in lower concentration of K^+ (10^{-7}–10^{-5} M) and high affinity sites with a stoichiometry of $n = 1.80 \pm 0.2$ in corresponding concentration of K^+ (10^{-4}–10^{-2} M). Significantly, two types of distinct metal binding modes to the G-quadruplex structure could be demonstrated as follows: A loose binding state arises in low concentration of K^+ and a tight binding state gradually appears with an increasing concentration of K^+. As shown in circular dichroism (CD) results, there are presenting different spectral intensity and two kinds of growth modes depending on the concentration of K^+ from 10^{-7} to 10^{-2} M (Figure S7, Supporting Information). The G-quadruplex structure is promoted in the presence of K^+ (0.1 and 0.2 M) to a folded saturated state, and it can be regarded as unfolded state in the absence of K^+. The CD spectra date indicates that the state transition between the different metal binding modes is induced by various concentrations of K^+. The results are consistent with the sequential multistates (folded, intermediate and unfolded) which exist in the complex formation process of a G-quadruplex structure, as described by Chaires and Vesnaver.[22]

Figure 4b shows the different redshifts of similar nanoaptasensors in different concentrations of K^+ solution. A linear relation between the $\Delta\lambda$ and the concentration of K^+ in the range of 10^{-7}–10^{-4} M is observed, which is then given by the following equation

$$f(\lambda) = 3.76 \lg C_{K^+} + 29.22 (R^2 = 0.9967) \quad (2)$$

The direct relation of the free energy change (ΔG) to the structural stability of the G-quadruplex structure is calculated at 25 °C using the following equations

$$f_u = \frac{(\lambda_1 - \lambda)}{(\lambda_1 - \lambda_2)} \quad (3)$$

$$K_{ep} = \frac{(1 - f_u)}{f_u} \quad (4)$$

$$\Delta G = -RT \ln K_{ep} \quad (5)$$

Here, f_u is the fraction of unfolded molecule, λ_1 and λ_2 are the values of the redshift of the LSPR spectra at the folded and unfolded states from the pre and posttransition baselines

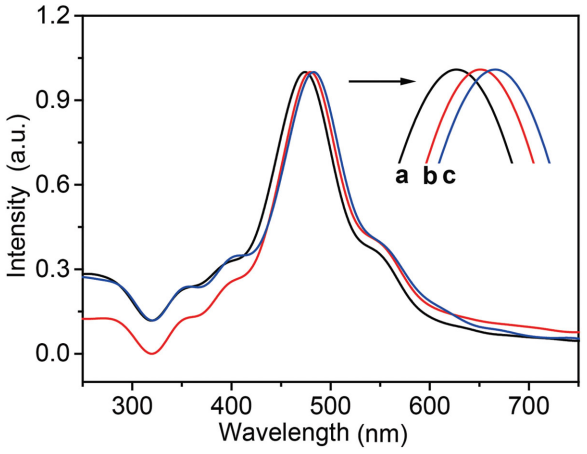

Figure 5. Extinction spectra of a) Au@Ag NCs solution, b) sensors solution, c) incubating sensors, and K^+ solution.

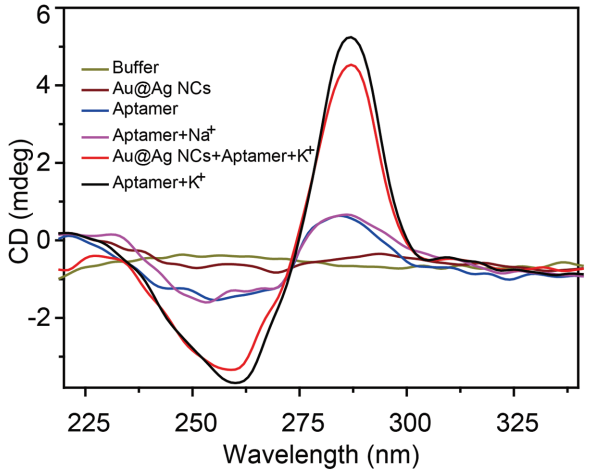

Figure 6. CD measurements of aptamer solutions containing Na^+ and K^+ before and after addition of Au@Ag NCs. [Aptamer] = 1×10^{-6} M; [NaCl] = [KCl] = 50×10^{-3} M.

at the different concentrations of K^+. K_{ep} is the equilibrium constant of the unfolding reaction. The free energy ΔG, as a linear function of K^+ concentration, can be fitted to the Equation (5) using a least-squares analysis, as shown in Figure 4c.

$$\Delta G = \Delta G_{H_2O} - mC_{K^+} \quad (6)$$

Here ΔG_{H_2O} is the free energy change of the folded G-quadruplex, and m is the solvent-exposed surface. As shown in Figure 4c, the ΔG value increases linearly with increasing concentration. The ΔG_{H_2O} = –24.46 kcal M^{-1} and m = 4.22 is close to the previous results.[11a,12a] These values of ΔG indicate that a higher concentration K^+ strengthens the conformational stability of the G-quadruplex structure.

2.4. Extinction Spectra Measurements

The sensor could be used not only at an individual particle level but also in bulk solution by UV–vis spectroscopy. **Figure 5** shows the extinction spectra of (a) the Au@Ag NCs solution, (b) sensors solution, and (c) sensors and K^+ solution, respectively. A full description of the experimental procedure can be found in the Supporting Information. Because the Au@Ag NCs have a different RI before and after modification of the aptamer, the aptamer on the surface of Au@Ag NCs leads to a LSPR spectra peak redshift from 473.5 to 479.8 nm; the formation of G-quartet complex on the surface in the presence of K^+ results in a further redshift from 479.8 to 483.2 nm. The LSPR scattering peak positions redshift notably when the RI of the local environment near the noble metals increases either in different solutions or on different substrates.[23] Compared with the extinction spectra of the Au@Ag NCs solution, the single nanoparticle scattering spectrum shows a larger redshift after immobilizing on the ITO glass slide.[24] These results are consistent with the LSPR results of the individual particle.

2.5. CD Measurements

The CD spectra provide reliable information for identifying DNA structures and are useful for characterizing the G-quadruplex structure. To further prove that the probe DNA molecules on the nanoaptasensor surface fold into a G-quadruplex structure in the K^+ solution, the CD spectra were employed to detect the folding process. The CD spectra of the aptamer in buffer were collected using a circular dichroism spectrometer. Three scans from 220 to 340 nm at 0.1-nm intervals were accumulated and averaged (see the Supporting Information for more details). The background of the buffer solution was subtracted from the CD data. As shown in **Figure 6**, the formation of G-quadruplex with the addition of K^+ is confirmed by CD analysis. The characteristic absorption bands near 260 and 290 nm of the quadruplex were observed only in the presence of K^+, as reported previously.[5c,11b,12b,25]

3. Conclusion

In summary, a simple, ultrasensitive and label-free plasmonic nanoaptasensor based on an individual nanoparticle is developed for real-time monitoring the conformational change of telomeric G-rich DNA to form the G-quadruplex, which can also be used as a K^+ nanoscale sensor with a lower limit of detection (LOD) (1×10^{-9} M) in a wide concentration range of 1×10^{-9}–10×10^{-3} M. The results indicate that there is a tiny RI change in the RIs before and after the G-quadruplex formation, and the RI change could be used for designing novel plasmonic sensors for label-free detection with high sensitivity. This work shows that the nanosensor is efficient for the study of aptamer and potassium ions interfacial interactions using LSPR. Furthermore, it also demonstrates that LSPR is a valid method to obtain the dissociation constants of the interactions (K_d) and the change in free energy (ΔG) of the telomeric aptamer. We demonstrate that there are two types of binding states in the sequential folding process, which is important to study the structural transition of G-quadruplex with thermostability. Accordingly, this plasmonic nanotechnique can be further explored for the sensing of other types of G-rich aptamer-binding and is promising for broad

potential applications in kinetics by monitoring the structural switch of the telomeric G-quadruplex.

4. Experimental Section

Materials: Oligonucleotides with specific sequences were synthesized by Sangon Biotech CO., LTD. (Shanghai, China). The sequence of oligonucleotide employed is: 5′-TTT TTT TTT TGG GTT AGG GTT AGG GTT AGG GTT TTT TTT TT-3′-$(CH_2)_6$–SH. Gold (III) chloride trihydrate ($HAuCl_4 \cdot 3H_2O$), silver nitrate ($AgNO_3$), sodium borohydride ($NaBH_4$), L-ascorbic acid (AA), cetyltrimethylammonium bromide (CTAB), and cetyltrimethylammonium chloride (CTAC) were all purchased from Sigma–Aldrich and used as received. All other chemicals were of analytical grade. All stock and buffer solutions were prepared with a Milli-Q ultrahigh-purity water system (Milli-Q, Millipore, US).

Dark-Field Condenser: The DFM imaging and SPR scattering spectrum measurements were carried out on an inverted microscope (eclipse Ti-U, Nikon, Japan) equipped with a dark field condenser ($0.8 < NA < 0.95$) and a 60× objective lens, a 100 W halogen lamp, a true-color digital camera (Nikon DS-fi2), and a monochromator (Acton SP2358) equipped with a spectrograph CCD (PIXIS 400BR: excelon, Princeton Instruments) and a grating (grating density: 300 L mm^{-1}; blazed wavelength: 500 nm). The spectra were integrated as 20 s with a 1 μm slit width.

ITO Glass Substrate Cleaning: For immobilization of the Au@Ag NCs onto the ITO glass substrate, the ITO glass substrate (3×1 cm, 8–12 Ω) was cleaned using lotion to remove organic residues, followed by sonication in acetone, ethanol, and ultrapure water for at least 120 min to remove excess blots, respectively. Then, the substrate was dried under a stream of N_2. Finally, the cleaned ITO glass slide was modified with the Au@Ag NCs by dipping in the diluted nanoparticle solution for 1 min, followed by rinsing with water to remove nonadsorbed Au@Ag NCs and drying under a stream of N_2.

Synthesis of Au@Ag NCs: Typically the Au seeds were synthesized using a two-step procedure: (i) small (2–3 nm) Au nanocrystallites were synthesized by reducing $HAuCl_4$ with $NaBH_4$ at the presence of CTAB, then (ii) these Au nanocrystallites were allowed to grow into Au nanocrystal seeds of 10 nm in size at the presence of additional $HAuCl_4$, AA, and CTAC. And repeat the step (ii) for preparation of 30 nm gold seeds (Figure S8, Supporting Information). The Au@Ag NCs with an edge length of ≈50 nm were formed by depositing Ag on the as-prepared CTAC-Au seeds. In typical synthesis, $AgNO_3$, AA, and CTAC were added into an aqueous suspension containing the Au seeds held at 60 °C. Cubic Au@Ag core-shell nanocrystals were formed due to the conformal over-growth of Ag on the CTAC-Au seeds. The edge lengths of the cubes can be finely controlled by injecting different volumes (0.1, 0.2, 0.4, 0.6, 0.8, and 1 mL) of $AgNO_3$ (0.01 M) into aqueous suspensions containing (13 mL) the same amount of Au seeds (Figure S1, Supporting Information). It can be seen that the edge lengths of the resultant Au@Ag cubes in TEM (JEM-1400, JEOL, Japan) images, which are very close to calculated results based on the number of Au seeds and the amount of $AgNO_3$ added (Figure S9, Supporting Information). [19]

Extinction Spectra and CD Measurements: The nucleic acid strands solution was heated to 60 °C and slowly cooled down to room temperature. This heating and cooling step helps to maintain the structural flexibility of the aptamer. After heating and cooling the aptamer solution as described above, the Au@Ag NCs solution was modified with the prepared aptamer solution to obtain the sensing solution. The sensor solution was prepared by 1×10^{-6} M aptamer containing about 0.1×10^{-9} M Au@Ag NCs in Buffer (10×10^{-3} M PBS, pH 7.4). Then, 2 mL sensor solution was added to potassium ions (1 M, 100 μL). Then, the resulting solution was incubated at 37 °C for 30 min to induce the aptamer to form G-quadruplex structures under the effect of potassium ion (Au@Ag@G-qus solutions). The prepared Au@Ag NCs solution, sensor solution, and Au@Ag@G-qus solutions were used for extinction spectra and CD measurements at room temperature. The aptamer stock solution (10×10^{-6} M, 200 μL) was added to 2 mL of buffer, and the resulting solution was incubated at 37 °C for 30 min in the presence or absence of potassium ions for CD measurements.

Supporting Information

Supporting Information is available from the Wiley Online Library or from the author.

Acknowledgements

Y.Y.T. and L.Z. contributed equally to this work. For the financial support for this work, the authors thank the National Basic Research Program of China (Grant No. 2012CB933301), the National Natural Science Foundation of China (Grant Nos. 61205195, 61571239, 21475064, 61378081, and 31200453), the Program for Changjiang Scholars and Innovative Research Team in University (IRT_15R37), the Specialized Research Fund for Doctoral College (Grant Nos. 20123223120011 and 20123223110007), the Synergetic Innovation Center for Organic Electronics and Information Displays, the Priority Academic Program Development of Jiangsu Higher Education Institutions, and the Natural Science Foundation of Jiangsu Province, China (BM2012010, NY211003).

[1] a) L. Guo, J. A. Jackman, H. H. Yang, P. Chen, N. J. Cho, D. H. Kim, *Nano Today* **2015**, *10*, 213; b) Y. T. Long, C. Jing, *Localized Surface Plasmon Resonance Based Nanobiosensors*, Springer, New York, **2014**; c) X. Huang, S. Neretina, M. A. El-Sayed, *Adv. Mater.* **2009**, *21*, 4880.

[2] a) S. K. Ghosh, T. Pal, *Chem. Rev.* **2007**, *107*, 4797; b) B. K. Gorityala, Z. Lu, M. L. Leow, J. Ma, X. W. Liu, *J. Am. Chem. Soc.* **2012**, *134*, 15229; c) J. N. Anker, W. P. Hall, O. Lyandres, N. C. Shah, J. Zhao, R. P. Van Duyne, *Nat. Mater.* **2008**, *7*, 442.

[3] a) J. R. Hao, B. Xiong, X. D. Chen, Y. He, E. S. Yeung, *Anal. Chem.* **2014**, *86*, 4663; b) M. A. Beuwer, M. W. Prins, P. Zijlstra, *Nano Lett.* **2015**, *15*, 3507; c) L. Rodriguez-Lorenzo, R. de la Rica, R. A. Alvarez-Puebla, L. M. Liz-Marzan, M. M. Stevens, *Nat. Mater.* **2012**, *11*, 604.

[4] a) C. Sonnichsen, B. M. Reinhard, J. Liphardt, A. P. Alivisatos, *Nat. Biotechnol.* **2005**, *23*, 741; b) I. Ament, J. Prasad, A. Henkel, S. Schmachtel, C. Sonnichsen, *Nano Lett.* **2012**, *12*, 1092; c) L. X. Qin, Y. Li, D. W. Li, C. Jing, B.-Q. Chen, W. Ma, A. Heyman,

O. Shoseyov, I. Willner, H. Tian, Y. T. Long, *Angew. Chem.* **2012**, *51*, 140.

[5] a) G. L. Liu, Y. T. Long, Y. Choi, T. Kang, L. P. Lee, *Nat. Methods* **2007**, *4*, 1015; b) Y. Choi, Y. Park, T. Kang, L. P. Lee, *Nat. Nanotechnol.* **2009**, *4*, 742; c) B. Kim, I. H. Jung, M. Kang, H. K. Shim, H. Y. Woo, *J. Am. Chem. Soc.* **2012**, *134*, 3133.

[6] a) L. Zhang, Y. Li, D. W. C. Li, Jing, X. Y. Chen, M. Lv, Q. Huang, Y. T. Long, I. Willner, *Angew. Chem.* **2011**, *50*, 6789; b) M. A. Schmidt, D. Y. Lei, L. Wondraczek, V. Nazabal, S. A. Maier, *Nat. Commun.* **2012**, *3*, 1108.

[7] a) Y. L. Hu, L. Zhang, Y. Zhang, B. Wang, Y. W. Wang, Q. L. Fan, W. Huang, L. H. Wang, *ACS Appl. Mater. Interfaces* **2015**, *7*, 2459; b) L. Zhang, Y. Zhang, Y. L. Hu, Q. L. Fan, W. J. Yang, A. R. Li, S. Z. Li, W. Huang, L. H. Wang, *Chem. Commun.* **2015**, *51*, 294; c) H. S. Cho, E. C. Yeh, R. Sinha, T. A. Laurence, J. P. Bearinger, L. P. Lee, *ACS Nano* **2012**, *6*, 7607; d) E. Martinsson, M. M. Shahjamali, N. Large, N. Zaraee, Y. Zhou, G. C. Schatz, C. A. Mirkin, D. Aili, *Small* **2016**, *12*, 330.

[8] H. Han, L. H. Hurley, *Trends Pharmacol. Sci.* **2000**, *21*, 136.

[9] a) J. T. Davis, *Angew. Chem.* **2004**, *43*, 668; b) M. Y. Kim, H. Vankayalapati, K. Shin-Ya, K. Wierzba, L. H. Hurley, *J. Am. Chem. Soc.* **2002**, *124*, 2098.

[10] a) T. Li, E. Wang, S. Dong, *Anal. Chem.* **2010**, *82*, 1515; b) J. M. Wilcox, D. L. Rempel, M. L. Gross, *Anal. Chem.* **2008**, *80*, 2365.

[11] a) B. I. Kankia, L. A. Marky, *J. Am. Chem. Soc.* **2001**, *123*, 10799; b) M. S. Choi, M. Yoon, J. O. Baeg, J. Kim, *Chem. Commun.* **2009**, *47*, 7419.

[12] a) P. Balagurumoorthy, S. K. Brahmachari, D. Mohanty, M. Bansal, V. Sasisekharan, *Nucleic Acids Res.* **1992**, *20*, 4061; b) K. N. Luu, A. T. Phan, V. Kuryavyi, L. Lacroix, D. J. J. Patel, *Am. Chem. Soc.* **2006**, *128*, 9963; c) H. C. Kuo, C. F. Cheng, R. B. Clark, J. J. C. Lin, J. L. C. Lin, M. Hoshijima, V. T. B. Nguyen-Tran, Y. S. Gu, Y. Ikeda, P. H. Chu, J. Ross, W. R. Giles, K. R. Chien, *Cell* **2001**, *107*, 801.

[13] a) Z. Chen, L. Chen, H. Ma, T. Zhou, X. Li, *Biosens. Bioelectron.* **2013**, *48*, 108; b) C. C. Huang, H. T. Chang, *Chem. Commun.* **2008**, *12*, 1461.

[14] Y. Xiao, A. A. Lubin, A. J. Heeger, K. W. Plaxco, *Angew. Chem.* **2005**, *117*, 5592.

[15] H. J. Lipps, D. Rhodes, *Trends Cell Biol.* **2009**, *19*, 414.

[16] a) P. K. Jain, K. S. Lee, I. H. El-Sayed, M. A. El-Sayed, *J. Phys. Chem. B* **2006**, *110*, 7238; b) P. K. Jain, X. H. Huang, I. H. El-Sayed, M. A. El-Sayed, *Acc. Chem. Res.* **2008**, *41*, 1578; c) Y. Zhao, Y. K. He, J. Zhang, F. B. Wang, K. Wang, X. H. Xia, *Chem. Commun.* **2014**, *50*, 5480.

[17] B. Xiong, R. Zhou, J. Hao, Y. Jia, Y. He, E. S. Yeung, *Nat. Commun* **2013**, *4*, 1.

[18] a) B. Sepulveda, P. C. Angelome, L. M. Lechuga, L. M. Liz-Marzan, *Nano Today* **2009**, *4*, 244; b) G. Nusz, A. Chilkoti, in *Nanoplasmonic Sensors*, Springer, New York **2012**.

[19] Y. Ma, W. Li, E. C. Cho, Z. Li, T. Yu, J. Zeng, Z. Xie, Y. Xia, *ACS Nano* **2010**, *4*, 6725.

[20] S. H. Im, Y. T. Lee, B. Wiley, Y. N. Xia, *Angew. Chem.* **2005**, *44*, 2154.

[21] R. E. Armstrong, G. F. Strouse, *Bioconjugate Chem.* **2014**, *25*, 1769.

[22] a) R. D. Gray, R. Buscaglia, J. B. Chaires, *J. Am. Chem. Soc.* **2012**, *134*, 16834; b) M. Bončina, J. Lah, I. Prislan, G. Vesnaver, *J. Am. Chem. Soc.* **2012**, *134*, 9657.

[23] A. D. McFarland, R. P. Van Duyne, *Nano Lett.* **2003**, *3*, 1057.

[24] a) E. Ringe, J. M. McMahon, K. Sohn, C. Cobley, Y. Xia, J. Huang, G. C. Schatz, L. D. Marks, R. P. Van Duyne, *J. Phys. Chem. C* **2010**, *114*, 12511; b) J. Becker, *Plasmons as Sensors*, Springer, Berlin, Germany **2012**.

[25] a) H. Qin, J. Ren, J. Wang, N. W. Luedtke, E. Wang, *Anal. Chem.* **2010**, *82*, 8356; b) E. M. Rezler, J. Seenisamy, S. Bashyam, M. Y. Kim, E. White, W. D. Wilson, L. H. Hurley, *J. Am. Chem. Soc.* **2005**, *127*, 9439.

Received: January 6, 2016
Revised: March 8, 2016
Published online: April 23, 2016